Proceedings of Australasian Conference on Robotics and Automation, 3-5 Dec 2012, Victoria University of Wellington, New Zealand.

Nonlinear Dynamic Modeling for High Performance Control of a Quadrotor

Moses Bangura, Robert Mahony
Australian National University, Canberra, Australia
Moses.Bangura@anu.edu.au, Robert.Mahony@anu.edu.au

Abstract

In this paper, we present a detailed dynamic and aerodynamic model of a quadrotor that can be used for path planning and control design of high performance, complex and aggressive manoeuvres without the need for iterative learning techniques. The accepted nonlinear dynamic quadrotor model is based on a thrust and torque model with constant thrust and torque coefficients derived from static thrust tests. Such a model is no longer valid when the vehicle undertakes dynamic manoeuvres that involve significant displacement velocities. We address this by proposing an implicit thrust model that incorporates the induced momentum effects associated with changing airflow through the rotor. The proposed model uses power as input to the system. To complete the model, we propose a hybrid dynamic model to account for the switching between different vortex ring states of the rotor.

1 Introduction

A quadrotor is an aerial vehicle with four rotor-motor assemblies that provide lift and controllability. For the standard design, the rotors are counter-rotating and are made of fixed pitch blades; no cyclic pitch and swashplates. Their light weight ($< 4kg$), reliability, robustness, ease of design and simple dynamics have made them a preferred test platform for aerial robotics research [Mahony *et al.*, 2012]. A typical quadrotor is shown in Figure 1.

The majority of papers on quadrotor modeling have used the same model introduced in the late nineties (see for example Pounds [Pounds *et al.*, 2004] and Bouabdallah [Bouabdallah *et al.*, 2004]). Thrust and torque of each rotor are modeled as static functions of the square of rotor speed. This model is based on the static thrust characteristics of the motor-rotor system and holds for near hovering flights [Martin and Salaün, 2010] as the effects of translational lift, blade flapping and changes in the advance ratio are negligible. Hoffmann et al. [Hoffman *et al.*, 2007] combined this model with the electrical properties of the motors in the design of different PID controllers. In Orsag [Orsag *et al.*, 2009], the authors proposed a purely aerodynamic approach based on Blade Element Theory and Momentum Theory to derive the thrust equation. A drawback of their method is that it is inefficient to determine the aerodynamic parameters of the blades on quadrotors. Most currently used quadrotor models have ignored the effect of drag. Derafa et al. [Derafa *et al.*, 2006] proposed a linear relationship between the drag force and the translational velocity of the vehicle. They however failed to look at the different types of drag and their effects at high velocities. Secondary aerodynamic effects of quadrotors are well known. One of these effects is blade flapping. It has been extensively studied in the literature [Mahony *et al.*, 2012]. To account for secondary aerodynamic effects, the authors of [Huang *et al.*, 2009] used the current model with controllers compensating for these effects in doing aggressive stall turns at high velocities. The well known fact that there is error in the current quadrotor dynamic model has made iterative learning techniques the most common way of designing controllers for aggressive manoeuvres. This is further evident in the high performance flights presented in Purwin [Purwin and D'Andrea, 2009], Lupashin [Lupashin *et al.*, 2010] and Mellinger [Mellinger *et al.*, 2012] which are based on iterative learning methods.

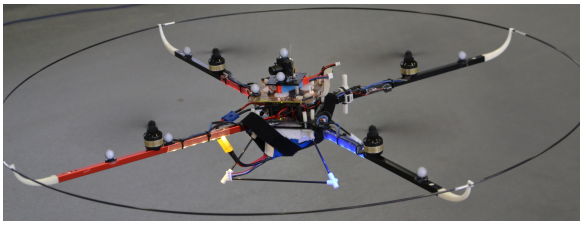

Figure 1: ANU Quadrotor.

In this paper, we propose a detailed dynamic and aerodynamic model for quadrotors that reduces modeling errors during high performance aggressive manoeuvres. In the model, we use mechanical power output from the motors as the free input to the vehicle. Due to the nonlinear mutual dependence of the aerodynamic and mechanical state of the vehicle, it is difficult to model the force/torque interaction using Newton-Euler formulation. It is however straightforward to model the relationship between mechanical power and aerodynamic power. Using Momentum Theory and the electrical properties of the motors, we derive equations outlining the use of mechanical power in the generation of exogenous forces: thrust and torque. In addition, we investigate and present models for the different types of drag forces acting on the vehicle as well as blade flapping. This leads to an explicit nonlinear state-space model of the quadrotor dynamics with free inputs that can easily be used for sophisticated control design such as Model Predictive Control (MPC). We also propose a hybrid dynamic model to account for the different operating states of a quadrotor in particular states associated with vertical descents.

The paper is organised as follows: the nonlinear dynamic equations are presented in Section 2 with power as input; Section 3 details the theoretical development of the concept of having power as input to the quadrotor; Section 4 outlines our proposed drag like forces; in Section 5, we propose a hybrid dynamic model to account for the different operating states of the vehicle and in Section 6 we illustrate usage of the model in a Nonlinear Model Predictive Control algorithm.

2 Nonlinear Equations of Motion

Consider the quadrotor shown in Figure 1. A quadrotor can be thought of as a rigid cross frame with four motor-rotor assemblies equidistance from the centre of gravity. The guidance and control system (Avionics, batteries and payload) are mounted above or below the intersection of the cross frames. Let $\{A\}$ denote the inertial frame and $\{B\}$ the body fixed frame. Let also (e_1, e_2, e_3) denote unit vectors in x_b, y_b and z_b directions. Before presenting the equations of motion, the following assumptions are made:

- The quadrotor is rigid and symmetrical about e_3 [Bouadi *et al.*, 2007].
- The centre of gravity is the origin of $\{B\}$ as suggested in Pounds [Pounds, 2007].

If the mass of the quadrotor (cross frame, batteries and payload) is m_{cg} and is centred at the centre of gravity, cylindrical about e_3 of radius r_{cg} and height h_{cg}. If h is the height of each rotor above the origin. If also m_r is the mass of each rotor with blades of radius r and chord length c, if also the mass of each motor is m_m, radius r_m and height h_m, then the mass moment of inertia $\mathbb{I} \in \mathbb{R}^{3\times3}$ of the quadrotor is

$$\mathbb{I}_{xx} = m_{cg}\frac{h_{cg}^2 + 3r_{cg}^2}{12} + 2m_m l^2 + 2\frac{1}{12}m_m(3r_m^2 + 4h_m^2) + 2m_r l^2 + 2\left(\frac{1}{12}m_r(2r)^2\right) \tag{1a}$$

$$\mathbb{I}_{yy} = m_{cg}\frac{h_{cg}^2 + 3r_{cg}^2}{12} + 2m_m l^2 + 2\frac{1}{12}m_m(3r_m^2 + 4h_m^2) + 2m_r l^2 + 2\left(\frac{1}{12}m_r c^2\right) \tag{1b}$$

$$\mathbb{I}_{xy} = \mathbb{I}_{yx} = 0 \tag{1c}$$

$$\mathbb{I}_{zz} = \frac{m_{cg}r_{cg}^2}{2} + 4m_m l^2 + 4\frac{m_m r_m^2}{2} + 4\frac{m_r\left((2r)^2 + c^2\right)}{12} + 4m_r l^2 \tag{1d}$$

$$\mathbb{I}_{xz} = \mathbb{I}_{yz} = \mathbb{I}_{zx} = \mathbb{I}_{zy} = 2m_m h_m l + 2m_r hl \tag{1e}$$

The quadrotor free body diagram and the different frames of references are shown in Figure 2.

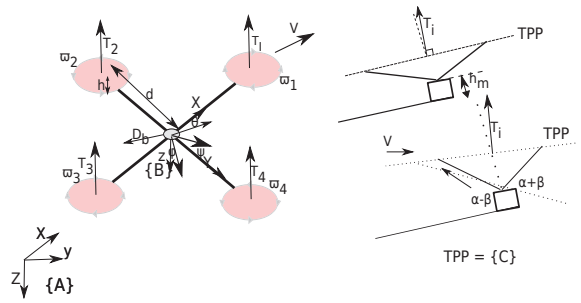

Figure 2: Free Body Diagram and Frames of Reference.

For notation, $\zeta = (x, y, z)^\top \in \{A\}$ the relative position of $\{B\}$ to the inertial frame $\{A\}$ and $V = (V_x, V_y, V_z)^\top \in \{B\}$ is the velocity of $\{B\}$ with respect to $\{A\}$. If the angular velocity of $\{B\}$ wrt $\{A\}$ is $\Omega = (\Omega_1, \Omega_2, \Omega_3)^\top \in \{B\}$ be the pitch, roll and yaw rates of the airframe measured in $\{B\}$, then the skew symmetric matrix $\Omega_\times$ is given by

$$\Omega_\times = \begin{pmatrix} 0 & -\Omega_3 & \Omega_2 \\ \Omega_3 & 0 & -\Omega_1 \\ -\Omega_2 & \Omega_1 & 0 \end{pmatrix}. \tag{2}$$

The kinematic equations are

$$\dot{\zeta} = V, \tag{3a}$$

$$\dot{R} = R\Omega_\times, \tag{3b}$$

We propose the use of mechanical power $P_m = P_{m_{i=1:4}}$ as control inputs (u) to the dynamics of the system. As will be shown in Section 3, the force F and torque τ, applied to the airframe, can be written as functions of the free input and the state of the system i.e. $F := F(V, \Omega, \varpi, P_m)$ and $\tau := \tau(V, \Omega, \varpi, P_m)$ respectively. Assuming the resultant torque generated by the weight of the motors and rotors to be zero and applying Newton's laws of motion, the dynamic equations of motion are shown in Equations 4a and 4b [Bouadi *et al.*, 2007], [Pounds *et al.*, 2006]

$$m\dot{V} = mge_3 - {}^B R_A^\top F(V, \Omega, \varpi, P_m)\, e_3 - {}^B R_A^\top D_b, \quad (4a)$$

$$\mathbb{I}\dot{\Omega} = -\Omega \times \mathbb{I}\Omega + G_a + \tau(V, \Omega, \varpi, P_m) + \tau_D, \quad (4b)$$

where $D_b \in \{B\}$ and $\tau_D \in \{B\}$ are the total drag force and torque associated with it (see Section 4 for details), G_a is the gyroscopic torque generated by the rotors as a result of rotation about the e_3 axis and the axis rotating at angular rates Ω of the quadrotor. The gyroscopic moment of the rotors on the airframe is ([Hamel *et al.*, 2002] and [Bouadi *et al.*, 2007])

$$G_a = -\sum_{i=1}^{4} (-1)^{i+1} \Omega_\times I_r \vec{\varpi}_i, \quad (5)$$

where

$$\vec{\varpi}_i = \begin{bmatrix} 0 \\ 0 \\ \varpi_i \end{bmatrix}$$

and $I_r \in \mathbb{R}^{3\times3}$ is the moment of inertia of the rotor. In reality, the thrust and torque from the motors are in the Tip Path Plane ($\{D\}$) of the rotors. Given the fact that the flapping angle β will be compensated for by the use of the flapping force presented in Section 4.1, we assume $\{C\} \equiv \{B\}$. Hence, $Fe_3 \in \{B\}$, $\tau \in \{B\}$ and the rotation representing the attitude of $\{A\}$ with respect to $\{B\}$, ${}^B R_A$ is denoted by $R \in \mathrm{SO}(3)$.

3 Using Power as a Free Input

This section introduces a model in which the power supplied to each motor is used as the free inputs to the system.

3.1 Motor Model

Brushless DC motors provide the mechanical power source for the quadrotor. The mechanical power output from each rotor is as a result of the electrical power it consumes from the battery. The electrical power consumed by a motor $P_{e_i} = V_{a_i} i_{a_i}$ is equal to the mechanical power $P_{m_i} = \tau_{z_i} \varpi_i$ minus power dissipated due to electrical resistance.

Ignoring the fast electrical dynamics of a motor, the rotor torque and applied voltage across a motor are modelled by [Franklin*et al.*, 2008]

$$V_{a_i} = K_e \varpi_i + R_a i_{a_i}, \quad (6a)$$

$$\tau_{z_i} = K_q i_{a_i}, \quad (6b)$$

where ϖ_i is the rotor speed, i_{a_i} is the current through the motor, R_a its electrical resistance and K_e and K_q are motor parameters. Using Equations 6a and 6b and the mechanical power $P_{m_i} = \tau_{z_i} \varpi_i$, one gets the following equation

$$P_{m_i} = \frac{K_q \varpi_i}{R_a} \left(V_{a_i} - K_e \varpi_i\right). \quad (7)$$

For a given desired power P_{m_i} this equation can be solved for the required voltage

$$V_{a_i} = \left(\frac{R_a P_{e_i}}{K_q \varpi_i} + K_e \varpi_i\right).$$

To obtain the PWM_i setting for a motor, one uses the standard relationship between average voltage and voltage of the battery as shown by

$$PWM_i = \left(\frac{V_{a_i}}{V_{source}}\right)^2,$$

where PWM_i is measured in fractions of cycle time.

3.2 Motor-Rotor System Identification

To determine the motor parameters and thrust and torque coefficients, a series of experiments were carried out as explained in Hoffman [Hoffman *et al.*, 2007]. The motor constants κ, K_q, K_e and R_a were obtained using linear regression. In determining the thrust coefficient C_T, a second order polynomial fit was used. The torque constant C_Q can then be determined using $C_Q = C_T/\kappa$. It should be noted that there is a quantisation error in the torque measurement which is evident for thrust inputs of $T = 2.5$ and $3N$. Figure 3(a) shows the variation of thrust with rotor speed ϖ, Figure 3(b) shows the thrust to torque variation from which C_Q could be determined. Figure 3(c) shows the linear relationship between electric current i_a and torque τ_z and Figure 3(d) shows the relationship between aerodynamic and mechanical power. The constant of proportionality between aerodynamic and mechanical power is the Figure of Merit (FoM). It is explained in Section 3.3. A summary of the results is shown in Table 1 and Figure 4 shows the experimental setup.

It should be noted that the C_Q and C_T determined from our static thrust tests are those used in thrust and torque models presented in Mahony [Mahony *et al.*, 2012] and Bouabdallah [Bouabdallah *et al.*, 2004] and are defined by

$$T_i = C_T \varpi_i^2,$$

and

$$\tau_{z_i} = C_Q \varpi_i^2.$$

In Section 3.5, it will be shown that the limiting case (near hover condition) of the proposed model is equivalent to the static model.

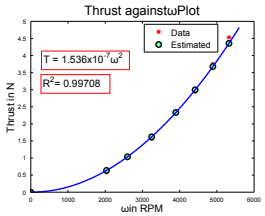

(a) Thrust and ϖ.

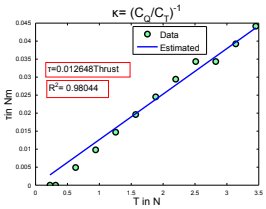

(b) Thrust and τ.

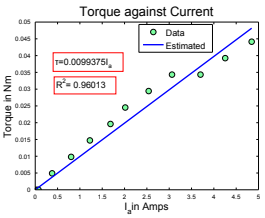

(c) τ and i_a.

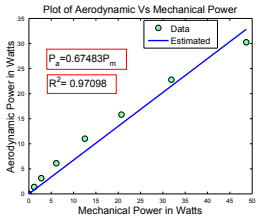

(d) FOM Plot.

Figure 3: Static Thrust Tests

Table 1: Static Thrust Experimental Values.

Name	Value	R^2
K_q	0.0099375	0.96013
K_e	0.0013	0.9978
R_a	0.5033	0.9978
FoM	0.67483	0.97098
C_T	1.536×10^{-7}	0.9971
κ	79.0660	0.98044

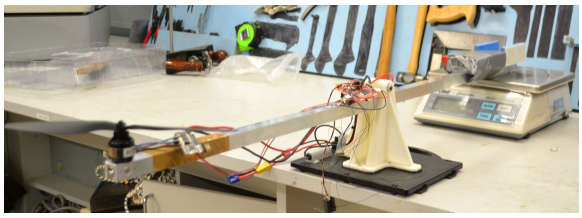

Figure 4: Static Thrust Test

3.3 Power Input

The connection between the mechanical power of the motors and aerodynamic power, that is associated with the aerodynamic forces (thrust and torque) generated, is given by the Figure of Merit (FoM). The FoM is a measure of the efficiency of the rotor blades in converting the mechanical power to aerodynamic (actual) power. The variation of C_T with advance ratio can be found in any rotary wing reference book or can be plotted using Blade Element Theory. At low forward velocities hence advance ratio, C_T is highest and the curve is flat. Combining this with the FoM variation with C_T shown in Leishman [Leishman, 2002] and for quadrotors with $\max .\varpi < 3\varpi_h$ and $V \leq 10$, one can assume a constant FoM.

The FoM relation between aerodynamic (P_a) and mechanical (P_m) power is given by [Leishman, 2002]

$$FoM = \frac{P_{a_i}}{P_{m_i}}. \tag{8}$$

3.4 Thrust on each Motor

Before presenting the thrust model, we compute the translational velocities of each rotor due to their distances from the centre of $\{B\}$ and rotational velocity Ω of the vehicle. The effective velocity $V_i \in \{B\}$ of each rotor is given by

$$\begin{aligned} V_1 &= V + \Omega_\times \left[de_1 - he_3 \right], \\ V_2 &= V + \Omega_\times \left[-de_2 - he_3 \right], \\ V_3 &= V + \Omega_\times \left[-de_1 - he_3 \right], \\ V_4 &= V + \Omega_\times \left[de_2 - he_3 \right], \end{aligned}$$

where V is the velocity of $\{B\}$ with respect to $\{A\}$ expressed in $\{B\}$, d and h are the distances and heights of the rotors from the centre of gravity.

Previous work involving the use of translational lift can be found in Hoffman [Hoffman *et al.*, 2007] and Leishman [Leishman, 2002]. Hoffman et al. [Hoffman *et al.*, 2007] calculated the thrust for various flight cases. They considered separate cases of translational, axial ascent and descent flights. This paper combines the effect of translational and axial flights as they are coupled during high performance and aggressive manoeuvres.

We use Momentum Theory to model both the static and translational lift produced by each rotor. Translational lift is extra lift generated as a result of translational motion of a rotor blade through air. As the rotor moves through the air, the vertical induced velocity of the air decreases while the horizontal component increases creating the additional lift (hence thrust) as illustrated in the control volume shown in Figure 5. This is a well known effect of rotor crafts and is well explained in references such as Leishman [Leishman, 2002] and Seddon [Seddon, 1990]. Using Momentum Theory, [Leishman, 2002] and [Seddon, 1990], the equations for

calculating thrust generated from the ith rotor as a result of the power imparted into the ensuing airflow are

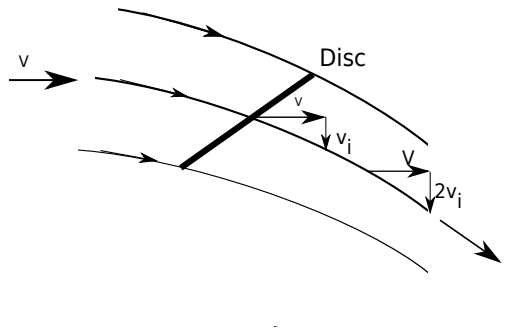

Figure 5: Induced Airflow Through a Rotor in Forward Flight.

$$T_i = 2\rho A v_{i_i} U_i, \tag{10a}$$
$$P_{a_i} = 2\rho A v_{i_i} U_i (v_{i_i} - V_{z_i}), \tag{10b}$$

where v_{i_i} is the induced vertical velocity through the rotor, $A = \pi r^2$ is the area of the rotor disk and the velocity at the rotor disk U_i is

$$U_i = \sqrt{V_{x_i}^2 + V_{y_i}^2 + (-V_{z_i} + v_{i_i})^2}. \tag{11}$$

Note the sign of V_{z_i} as z is positive downwards whereas v_{i_i} is positive upwards.

This additional lift which increases the effective thrust has an associated drag known as Translational Drag and is discussed in Section 4.3.

To compute the thrust generated by rotor i for a given aerodynamic power P_{a_i}, one must solve Equation 10b and 11 to compute the induced velocity v_{i_i}. This is done by using Newton's iterative method comparing the calculated to the given aerodynamic power. This induced velocity v_{i_i} is then used in Equation 10a to compute the thrust T_i.

3.5 Resolving the Rigid-body Force and Torque

If the thrust generated by a rotor is $T_i := T_i\left(V_i, \Omega, \varpi_i, P_{m_i}\right)$, the resultant thrust force from all four rotors is given by

$$F = \sum_{i=1}^{4} T_i. \tag{12}$$

The moment created by each thrust force about x y-axis is presented by

$$\tau_{x,y} = \begin{pmatrix} 0 & -d & 0 & d \\ d & 0 & -d & 0 \end{pmatrix} \begin{pmatrix} T_1 \\ T_2 \\ T_3 \\ T_4 \end{pmatrix}. \tag{13}$$

One should note that though the rotors are at a height h above the origin, the moments due to the thrust T_i is unaffected by this e_3 shift. It can be shown that the current through a motor is given by

$$i_{a_i} = \frac{P_{m_i}}{K_q \varpi_i}.$$

From the model proposed in Section 3.1, the torque from the motors are determined based on their mechanical power output. Therefore τ_z is given by

$$\tau_z = \begin{pmatrix} K_q & -K_q & K_q & -K_q \end{pmatrix} \begin{pmatrix} i_{a_1} \\ i_{a_2} \\ i_{a_3} \\ i_{a_4} \end{pmatrix}. \tag{14}$$

Substituting for the currents, Equation 14 can be rewritten as

$$\tau_z = \begin{pmatrix} \frac{K_q}{\varpi_1} & -\frac{K_q}{\varpi_2} & \frac{K_q}{\varpi_3} & -\frac{K_q}{\varpi_4} \end{pmatrix} \begin{pmatrix} P_{m_1} \\ P_{m_2} \\ P_{m_3} \\ P_{m_4} \end{pmatrix}. \tag{15}$$

In the limiting case, at hover, $\Omega, V = 0$, one can deduce $U_i = v_{i_i} = v_h$, $T_i = 2\rho A v_{i_i}^2 = \frac{mg}{4}$, $P_{a_i} = 2\rho A v_{i_i}^3$, $D_b = 0$, $G_a = 0$, $\tau_D = 0$, $\tau_{z_i} = \frac{T_i}{\kappa}$, $\kappa = \frac{T_i}{\tau_{z_i}} = \frac{C_T}{C_Q}$ $P_{m_i} = \frac{P_{a_i}}{FoM}$ of each rotor

$$\varpi_i = \frac{P_{m_i}}{\tau}$$

Substituting values, one recovers the static thrust model $T_i = C_T \varpi_i^2$.

4 Drag Like Effects

Drag is that force that opposes the motion of an object in air subject to an applied force. Classical drag models ([Leishman, 2002], [Bramwell *et al.*, 2001] and [Seddon, 1990]) developed for full scale rotary wing aircrafts are based on steady-state forward flight conditions and are primarily developed with the goal of computing the efficiency of flight regimes rather than modeling system dynamics. A major shortcoming of the classical models is that at hover, they predict a significant residual drag. The approach taken in the sequel is targeted towards providing a simple lumped parameter nonlinear model for quadrotor dynamics. In particular, we will treat blade flapping as a drag-like force (that opposes the motion of the vehicle), rather than the classical treatment for rotor craft where it is incorporated into cyclic

rotor pitch models as an offset. In addition, we consider induced drag associated with rigidity of the rotor, something that is far more significant for small quad rotors than for full scale rotor crafts. Finally, classical translational drag and parasitic drag effects are modeled in a way that is valid over the full vehicle flight envelope - not just for steady-state forward flight.

4.1 Blade Flapping

Blade flapping is a phenomenon that occurs when rotor blades undergo translational motion. During the motion, the advancing blade experiences a higher tip velocity creating an increase in lift while the retreating blade experiences a reduction in tip velocity and therefore a reduction in lift as shown in Figure 2. The differential lift applies a torque to the heavily damped spinning rotor disk that leads to a gyroscopic response that tilts the rotor disk back, reducing the advancing angle of attack and increasing the retreating angle of attack, until the rotor reaches aerodynamic equilibrium and the aerodynamic forces on the rotor are balanced. The resulting rotor tip path flaps up relative to the rotor mast as the blade is advancing and flaps down as the blade is retreating. The angle through which the rotor tip path plane (TPP) is deflected is the flapping angle, β.

The tip path plane of the rotor can be modeled as a flapping angle $\beta(\psi)$ written as a function of azimuth angle ψ [Leishman, 2002]

$$\beta(\psi) = \beta_0 + \beta_c \cos(\psi) + \beta_s \sin(\psi). \tag{16}$$

Detailed models of the constants β_c and β_s, that also include dependence on angular velocities of the airframe, are provided by Pounds [Pounds, 2007]

$$\beta_c = \frac{-\mu A_{1c}}{1-\frac{1}{2}\mu^2} + \frac{\frac{-\frac{16}{\gamma}(\frac{\Omega_1}{\varpi})}{(1-\frac{e}{r})^2} + (\frac{\Omega_2}{\varpi})}{1-\frac{\mu^2}{2}} + \frac{\frac{\frac{12}{\gamma}\frac{e}{r}}{(1-\frac{e}{r})^3}\left[\frac{-\frac{16}{\gamma}(\frac{\Omega_2}{\varpi})}{(1-\frac{e}{r})^2} - \frac{\Omega_1}{\varpi}\right]}{1-\frac{\mu^4}{4}} \tag{17}$$

and

$$\beta_s = \frac{-\mu A_{1s}}{1+\frac{1}{2}\mu^2} + \frac{\frac{-\frac{16}{\gamma}(\frac{\Omega_2}{\varpi})}{(1-\frac{e}{r})^2} + (\frac{\Omega_1}{\varpi})}{1-\frac{\mu^2}{2}} + \frac{\frac{\frac{12}{\gamma}\frac{e}{r}}{(1-\frac{e}{r})^3}\left[\frac{-\frac{16}{\gamma}(\frac{\Omega_1}{\varpi})}{(1-\frac{e}{r})^2} - \frac{\Omega_2}{\varpi}\right]}{1-\frac{\mu^2}{4}}, \tag{18}$$

where A_{1c} and A_{1s} are constants depending on blade geometry (Equation 4.45 and Equation 4.47 in [Leishman, 2002]),

$$\mu = \frac{|V_p|}{\varpi r}$$

is the advance ratio, the ratio of horizontal velocity of the vehicle to the rotor tip velocity and $V_p = \begin{pmatrix} V_x & V_y & 0 \end{pmatrix}^\top \in \{B\}$ is the velocity in the $x-y$ plane. The Lock Number which is between 2 and 20 is given by

$$\gamma = \frac{\rho a c r^4}{I_b}$$

where I_b is the rotational moment of inertia of the blade about the vertical flapping hinge e, c is chord length, a is the lift gradient of the aerofoil which can be assumed to be 2π [Anderson, 2007].

With μ very small so that $\mu^2 \approx 0$ and splitting Equation 17 and 18 into components due to linear and angular velocities, one obtains

$$\beta_c = \frac{-|V_p|}{\varpi r} A_{1c} - \frac{1}{\varpi} B_2 \Omega_1 + \frac{1}{\varpi} B_1 \Omega_2, \tag{19}$$

and

$$\beta_s = \frac{-|V_p|}{\varpi r} A_{1s} + \frac{1}{\varpi} B_1 \Omega_1 - \frac{1}{\varpi} B_2 \Omega_2. \tag{20}$$

If we let

$$A_{flap} = \frac{1}{r}\begin{pmatrix} -A_{1c} & A_{1s} & 0 \\ -A_{1s} & -A_{1c} & 0 \\ 0 & 0 & 0 \end{pmatrix} \tag{21}$$

and

$$B_{flap} = \begin{pmatrix} -B_2 & B_1 & 0 \\ B_1 & -B_2 & 0 \\ 0 & 0 & 0 \end{pmatrix}, \tag{22}$$

be lumped parameter matrices that must be identified from flight tests, then Equation 19 and 20 can be rewritten in a lumped parameter form to obtain the flapping force on a rotor i as [Mahony *et al.*, 2012]

$$\Delta_i = T_i \left(A_{flap} \frac{V_{p_i}}{\varpi_i} + B_{flap} \frac{\Omega}{\varpi_i} \right). \tag{23}$$

4.2 Induced Drag

If the blades are semirigid or fully rigid, they do not flap freely to obtain the aerodynamic balance of forces. This causes an effect on the airframe termed induced drag. For a rotor that is mechanically stiff, blade flapping is unable to fully compensate for the thrust imbalance on the rotor and the advancing blade generates more lift than the retreating blade. For any aerofoil that generates lift (in our case the rotor blade as it rotates around the rotor mast), there is an associated instantaneous induced drag due to the backward inclination of aerodynamic force with respect to the aerofoil motion. The instantaneous induced drag is proportional to the instantaneous lift generated by the aerofoil. In normal hover conditions for a rotor, the instantaneous induced drag is constant through all azimuth angles of the rotor and is directly responsible for the aerodynamic torque τ_z. However, when there is a thrust imbalance, then the sector of the rotor traveling with high thrust (for the advancing rotor) will generate more induced drag than the sector where the rotor generates less thrust (for the retreating blade). The net result will be that the rotor experiences a net instantaneous induced drag that directly opposes the direction of apparent wind as seen by

the rotor and that is proportional to the velocity of the apparent wind.

$$D_I = K_I V_p, \quad V_p = (V_x, V_y, 0)^\top .$$

This effect is often negligible for full scale rotor crafts since the mechanical flexibility of the blade is insignificant compared to the aerodynamic forces. However, it may be quite significant for small quadrotor vehicles with relatively rigid blades.

The consequence of blade flapping and induced drag taken together ensures that there is always a noticeable horizontal drag experienced by a quadrotor even when manoeuvering at relatively slow speeds.

4.3 Translational Drag

This is otherwise known as momentum drag described in Pflimlim [Pflimlin *et al.*, 2010]. It is drag caused by the induced velocity of the airflow as it goes through the rotor. Recall Figure 5 and note that the induced lift was associated with the redirection (in a downwards direction) of the airflow through the rotor. This process is similar to the way in which a traditional aerofoil redirects air downwards in level flight. In the same way that aerofoils generate induced drag, a rotor in forward flight also generates induced drag in proportion to the induced lift generated. If $V_p = (V_x, V_y, 0)^\top \in \{B\}$ is the velocity of the rotor on the x-y plane expressed in the body-fixed frame, the models we propose are given by

$$D_T = K_{T_1} V_P,$$

for low speed and

$$D_T = K_{T_2}(-V_z + v_i)^4 V_p,$$

for high velocities (where $V_p > w$, w is a constant velocity depending on the rotor) and are independent of rotor speed [Pflimlin *et al.*, 2010].

The models for both low and high velocities can be verified using the lift induced drag component ($\mathrm{dD_T} = \phi \mathrm{dL}$) from Blade Element Theory (BET) [Leishman, 2002].

4.4 Profile Drag

This is the drag caused by the transverse velocity of the rotor blades as they move through the air. It is zero at hover since the opposing forces generated on either side of the rotor hub are equal in magnitude. It is usually unaffected by the angle of attack of the blades' aerofoil and only slightly increases with airspeed.

It can be easily shown using Blade Element Theory (BET) that the profile drag is given by

$$D_p = \rho c \left(\left(c_{d0} + c_{d\alpha}\theta_0 \right) \Omega r^2 - (-V_z + v_i) r \right) V_p. \quad (24)$$

Moving vertically upwards, does not change the symmetry of the blades. This is seen in the equation as increasing the rate of climb ($-V_z$) requires increasing ϖ which will cause a reduction in v_i hence the overall effect is negligible. Increasing the planar velocity decreases v_i, increases the variation of flow variation across the rotor and therefore increases D_p. Using a lumped parameter K_p, we propose a linear variation of profile drag dependence on the forward speed.

$$D_p = K_p V_p \quad (25)$$

4.5 Parasitic Drag

This is the drag incurred as a result of the nonlifting surfaces of the quadrotor. It includes drag arising from the airframe, motors and the guidance and control system at the centre of the airframe. It is quite significant at high speeds for full sized rotor craft and becomes the predominant resistant force. For the flight envelope of quadrotor vehicles flying at moderate speeds up to $10m/s$, parasitic drag may often be ignored.

It is modeled by [Seddon, 1990]

$$D_{par} = K_{par}|V|V, \quad (26)$$

where $V = (V_x, V_y, V_z)^\top$, $K_{par} = \frac{1}{2}\rho S C_{D_{par}}$. Usually, $C_{D_{par}} <<< C_D$ of the rotor blades.

4.6 Drag Summary

The different drag models for variation of airspeed are shown in Figure 6. In summary, the drag model for a rotor i on a quadrotor is given by

$$D_i = D_{I_i} + D_{T_i} + D_{p_i} + \Delta_i.$$

Hence for low velocity manoeuvres one has,

$$\begin{aligned} D_i &= K_I V_{p_i} + K_T V_{p_i} + K_p V_{p_i} + A_{flap}\frac{V_{p_i}}{\varpi_i} + B_{flap}\frac{\Omega}{\varpi_i}, \\ &= D_K V_{p_i} + A_{flap}\frac{V_{p_i}}{\varpi_i} + B_{flap}\frac{\Omega}{\varpi_i}, \end{aligned} \quad (27)$$

where $D_K = K_I + K_T + K_p$. For high velocity manoeuvres where $V_p > w$, then

$$\begin{aligned} D_i = K_I V_{p_i} + K_{T_2}(-V_{z_i} + v_{i_i})^4 V_{p_i} + K_p V_{p_i} + \\ A_{flap}\frac{V_{p_i}}{\varpi_i} + B_{flap}\frac{\Omega}{\varpi_i} \end{aligned}$$

and hence

$$\begin{aligned} D_i = \left(K_I + K_p + K_{T_2}(-V_{z_i} + v_{i_i})^4 + A_{flap}\frac{1}{\varpi_i} \right) V_{p_i} \\ + B_{flap}\frac{\Omega}{\varpi_i} \end{aligned}$$

The total drag force acting on the vehicle is given by

$$D_b = \sum_{i=1}^{4} D_i + K_{par}|V|V \ \in \{B\}. \tag{28}$$

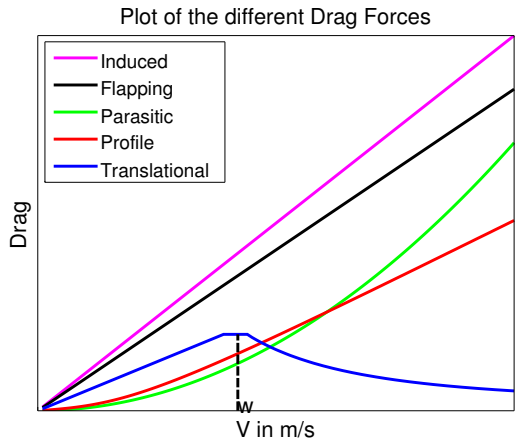

Figure 6: Relative Drag Variation with V.

Torque is created on the airframe by each of the drag forces (except for parasitic drag) due to their displacement offsets from the centre of gravity of the quadrotor. Hence the torque generated by the drag forces on each rotor is given by

$$\begin{aligned}
\tau_{D_1} &= D_1 \times [de_1 - he_3], \\
\tau_{D_2} &= D_2 \times [-de_2 - he_3], \\
\tau_{D_3} &= D_3 \times [-de_1 - he_3], \\
\tau_{D_4} &= D_4 \times [de_2 - he_3].
\end{aligned}$$

The total additional torque on the quadrotor as a result of drag forces on individual rotors is given by

$$\tau_D = \sum_{i=1}^{4} \tau_{D_i}. \tag{30}$$

5 Other Aerodynamic Effects

For flying quadrotors, two additional aerodynamic effects have been observed, ground effect and vortex ring states. Conditions under which these effects occur are presented in the subsections that follow. Prior to this section, the models presented are for what we refer to as the "normal operation" state.

5.1 Ground Effect

This has been observed for constant powered flights that are close to the ground. From Momentum Theory, the induced velocity v_i is a function of the length of the control volume. The presence of the ground causes a velocity of zero. This is transferred to the rotor disc through pressure changes in the wake resulting in lower induced velocity. This implies that the power required to hover close to the ground is lower than that far above it [Seddon, 1990].

The ratio of the thrust within and out of the ground cushion for a constant power flight is given by

$$\frac{T_g}{T_\infty} = \frac{1}{1 - \left(\frac{r}{4|z|}\right)^2 \left\{\frac{1}{1+\left(\frac{|V|}{v_i}\right)^2}\right\}} \tag{31}$$

where $|z|$ is the height above the ground, r is the radius of the rotor, T_g and T_∞ are the thrust within and out of the ground cushion [Cheeseman and Bennet, 1957]. It can be seen from Equation 31, that if $\frac{r}{|z|} > 0.1$, the ground effect diminishes. This indicates that ground effect becomes more significant with the size of the rotors. For quadrotors it is reasonable that the whole of the rotor area, and not just individual rotors, should be considered, although no experimental data on this is available.

5.2 Vertical Descent

During vertical descent flights, the climb velocity becomes negative while the induced velocity v_i remains positive. At higher descent rates, stronger tip vortices are accumulated close to the rotor plane causing sharp vibrations and uncommanded pitch and roll of the quadrotor. As the descent rate increases to multiples of the the induced velocity, the flight behaviour changes from "normal operating" state to Vortex Ring State (VRS), Turbulent Wake State (TWS) and eventually Windmill Brake State (WBS). It should be noted that flights within VRS and TWS cannot be modelled using Momentum Theory due to energy dissipation in the unsteady flow.

VRS is the first of these states. It occurs when the rate of descent is equal to half the induced velocity at hover (v_h). To recover from this state, more power needs to be supplied to the motors. This will reduce the rate of descent and blow away the vortex.

TWS occurs when the rate of descent equals that of the induced velocity. With this equality, there is no net flow of air through the rotor disc. Momentum theory predicts the nonexistence of thrust and therefore cannot be used. The vibrations are less in this state compared to those of VRS. To exit this state, additional power from the motors is required. This ensures that the vortex is blown away and the descent rate is decreased.

WBS occurs when the rate of descent is greater than twice the induced velocity at hover ($2v_h$). This causes the flow to be upwards throughout the entirety of the rotor creating a transfer of power to the air unlike the previous two states. The thrust generated by a rotor under this state is given by $T_i = -2\rho A(-V_{z_i} + v_{i_i})v_{i_i}$.

The induced velocity relates to v_h through $v_{i_i}(-V_{z_i} + v_{i_i}) = -v_h^2$ [Seddon, 1990].

To account for the different flight states of the vehicle, we propose a hybrid dynamic model shown in Table 2.

Table 2: Hybrid Dynamic States.

State	Condition	Model
Normal	$\frac{r}{\lvert z\rvert} > 0.1,\ -V_z < \frac{1}{2}v_h$	MT
VRS	$\frac{1}{2}v_h \leq -V_z < v_h$	
TWS	$v_h \leq -V_z < 2v_h$	
WBS	$-V_z \geq 2v_h$	MT
Ground Effect	$\frac{r}{\lvert z\rvert} \leq 0.1$	$\frac{T_g}{T_\infty}$

6 Model in Control Applications

To test the potential of the model presented in the paper, it is used in a Nonlinear Model Predictive Control (NMPC) algorithm for position control of a quadrotor. The approach taken is based on work presented in Grune et al. [Grune and Pannek, 2011] and the hybrid technique in Bemporard [Bemporad and Morari, 1999] to account for the various switching states of the vehicle.

1. Get a measurement of the state $(x = (\zeta, V, \Omega, R)^\top \in \mathbb{X})$ $x(n)$ for the current time $t = n$.
2. Use the measurement as initial value $x_0 \doteqdot x(n)$ to solve the optimal control problem

$$V^*(x_n) = \min_{u^*(.)\in\mathbb{U}} J_N(x_0, u(.)) \doteqdot \sum_{k=0}^{N-1} l\left(x_u(k, x_0), u(k)\right)$$

subject to:

$$\begin{aligned} x_u(0, x_0) &= x_0 \\ \dot{x} &= f(x, u) \\ u_{min} \leq u &\leq u_{max} \\ x_{min} \leq x &\leq x_{max} \end{aligned}$$

and obtain the optimal control sequence $u^*(.) \in \mathbb{U}^N(x_0)$

3. The NMPC-feedback value $\mu_N(x(n)) \doteqdot u^*(1) \in \mathbb{U}$ is added to past control moves
4. Use $u = \mu_N(x(n))$ along with $x(n)$ in the dynamic and kinematic equations presented in Section 2 i.e. $\dot{x} = f(x, u)$ and an appropriate integration technique to obtain the closed-loop response of the system $(x(n+1))$. Restart with $x_n = x_{n+1}$ [Grune and Pannek, 2011].

where N is the optimisation horizon, the running cost $l\left(x_u(k, x_0), u(k)\right) = (x - x_d)^\top P(x - x_d) + (u - u_h)^\top Q(u - u_h)$ and $P, Q \succeq 0$, the states $x = (\zeta, V, \Omega, R)^\top \in \mathbb{X}$, $x_d = (V_0, \zeta_d, \Omega_0, R_0)^\top \in \mathbb{X}$, subscript 0 implies element values are zero and control $u = (P_{m_1}, P_{m_2}, P_{m_3}, P_{m_4})^\top \in \mathbb{U}$ and power required to hover, $u_h = (P_{m_h}, P_{m_h}, P_{m_h}, P_{m_h})^\top$.

The results of the NMPC for a commanded position of $\zeta_d = (5, 5, -10)$ from $\zeta = (0, 0, -5)$ are shown in Figure 7(a) to 7(d). They are for a Mikrokopter quadrotor used by the ANU with values of $N = 10$, $P = I_{12\times12}$, $Q = 10^{-3}I_4$, $P_{m_{max}} = 90W$ as max. $P_e = 120$.

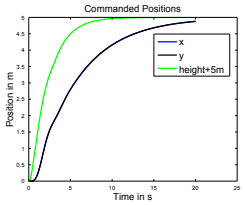

(a) Commanded Position.

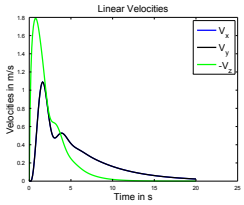

(b) Linear Velocities.

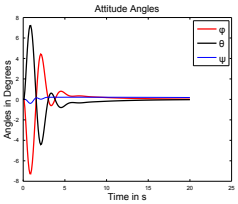

(c) Attitude Angles.

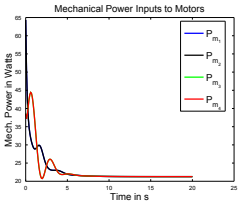

(d) Mech. Power Input.

Figure 7: NMPC Position Control

The simulation shown demonstrates that the NMPC algorithm can effectively deal with the proposed model and yields a controller that leads to stable and near optimal response of the simulated vehicle. Since the model includes secondary aerodynamic effects that are incorporated into the NMPC horizon the overall performance of the closed-loop system is expected to be superior to control based on the currently accepted model, at least in aggressive flight scenarios where these effects become significant. The response of the closed-loop system can be further improved by tuning the weighting parameters P and R in the NMPC design.

7 Conclusion

In this paper, we presented a detailed nonlinear dynamic model for high performance control of a quadrotor. The model uses mechanical power output from the rotors as inputs to the dynamics enabling the interaction of the mechanical and aerodynamic characteristics of the rotors to be accounted for. A detailed investigation and models of the drag forces acting on the vehicle was presented. To account for the different vortex ring states

of the vehicle, we proposed a hybrid dynamic system for switching between states. With this model, high performance control in particular MPC method as shown of a quadrotor can be carried out without the need for an iterative learning scheme or controllers to compensate for model errors.

References

[Leishman, 2002] J G Leishman. *Principles of Helicopter Aerodynamics,* Cambridge Aerospace Series, 2002.

[Seddon, 1990] John Seddon. *Basic Helicopter Aerodynamics,* BSP Professional Books, 1990.

[Bramwell *et al.*, 2001] A. R. S Bramwell, George Done and David Balmford. *Bramwell's Helicopter Dynamics,* AIAA Butterworth-Heinemann, 2nd ed., 2001.

[Hoffman *et al.*, 2007] Gabriel M. Hoffman, Haomiao Huang, Steven L. Waslander and Claire J. Tomlin. *Quadrotor Helicopter Flight Dynamics and Control: Theory and Experiment,* AIAA, 2007.

[Pounds *et al.*, 2004] Paul Pounds, Robert Mahony and Joeal Gresham. *Towards Dynamically-Favourable Quad-Rotor Aerial Robots,* Australasian Conference on Robotics and Automation, ACRA 2004.

[Pounds *et al.*, 2006] Paul Pounds, Robert Mahony and Peter Corke. *Modelling and control of a large quadrotor robot,* Australasian Conference on Robotics and Automation, ACRA 2006.

[Pounds, 2007] Paul Pounds. *Construction and Control of a Large Quadrotor Micro Air Vehicle,* ANU PhD Thesis, September 2007.

[Bouabdallah *et al.*, 2004] Samir Bouabdallah, Pierpaolo Murrieri and Roland Siegwart. *Design and Control of an Indoor Quadrotor,* Robotics and Automation, 2004.

[Hamel *et al.*, 2002] Tarek Hamel, Robert Mahony, Rogelio Lozano and James Ostrowski. *Dynamic Modelling and Configuration Stabilization for an X4-Flyer,* IFAC 15th Trienial World Congress, 2002.

[Bouadi *et al.*, 2007] H. Bouadi, M. Bouchoucha and M. Tadjine. *Modelling and Stabilizing Control Laws Design Based on Sliding Mode for an UAV Type-Quadrotor,* Engineering Letters, Nov. 2007.

[Huang *et al.*, 2009] Haomiao Huang, Gabriel M. Hoffman, Steven L. Waslander and Claire J. Tomlin. *Aerodynamics and Control of Autonomous Quadrotor Helicopters in Aggressive Maneuvering,* International Conference on Robotics and Automation, 2009.

[Mahony *et al.*, 2012] Robert Mahony, Vijay Kumar and Peter Corke. *Modelling, Estimation and Control of Quadrotor Aerial Vehicles,* Robotics and Automation Magazine, 2012.

[Martin and Salaün, 2010] Philippe Martin and Erwan Salan. *The True Role of Accelerometer Feedback in Quadrotor Control,* International Conference on Robotics and Automation, 2010.

[Derafa *et al.*, 2006] L. Derafa, T. Madani and A. Benallegue. *Dynamic Modelling and Experimental Identification of Four Rotors Helicopter Parameters,* IEEE Conf. on Industrial Technology, 2006.

[Orsag *et al.*, 2009] M. Orsag and S. Bogdan. *Hybrid Control of Quadrotor,* 17th Mediterranean Conf. on Control and Automation, 2009.

[Purwin and D'Andrea, 2009] Oliver Purwin and Raffaello DAndrea. *Performing Aggressive Maneuvers using Iterative Learning Control,* International Conference on Robotics and Automation, 2009.

[Lupashin *et al.*, 2010] S. Lupashin, A. Schollig, M. Sherback and Raffaello DAndrea. *A Simple Learning Strategy for High-Speed Quadrotor Multi-Flips,* International Conference on Robotics and Automation, 2010.

[Mellinger *et al.*, 2012] Daniel Mellinger, N. Michael and Vijay Kumar. *Trajectory generation and control for precise aggressive Maneuvers with quadrotors,* The International Journal of Robotics Research, 2012.

[Anderson, 2007] John D. Anderson. *Fundamentals of Aerodynamics,* The McGraw Hill Companies, Fourth edition, 2007.

[Franklin*et al.*, 2008] Gene F. Franklin, J. David Powell and Abbas Emani-Naeini. *Feedback Control of Dynamic Systems,* Pearson Education, 2008, 5th ed.

[Pflimlin *et al.*, 2010] J.-M. Pflimlin, P. Binetti, P. Soures, T. Hamelc, and D. Trouchet. *Modeling and attitude control analysis of a ducted-fan micro aerial vehicle,* Control Engineering Practice, 2010.

[Cheeseman and Bennet, 1957] I. C. Cheeseman and W. E. Bennet. *The effect of the ground on a helicopter rotor,* A.R.C Technical Report R & M No. 3021, 1957.

[Grune and Pannek, 2011] Lars Grüne and Jürgen Pannek. *Nonlinear Model Predictive Control: Theory and Algorithms,* Springer: Communications and Control Engineering, April 2011.

[Bemporad and Morari, 1999] Bemporad A. and Morari M. *Control of systems integrating logic, dynamics, and constraints* Automatica, 1999.